Journal of Alloys and Compounds 480 (2009) 152–156

Contents lists available at ScienceDirect

Journal of Alloys and Compounds

journal homepage: www.elsevier.com/locate/jallcom

Low-temperature thermal expansion of metastable intermetallic Fe–Cr phases

A. Gorbunoff[a,*], A.A. Levin[b], D.C. Meyer[b]

[a] University of Applied Sciences (HTW) Dresden, Friedrich-List-Platz 1, 01069 Dresden, Germany
[b] Institut für Strukturphysik, Technische Universität Dresden, 01062 Dresden, Germany

ARTICLE INFO

Article history:
Received 4 July 2008
Received in revised form
19 September 2008
Accepted 6 October 2008
Available online 4 December 2008

PACS:
61.05.cp
61.66.Dk
64.60.My
65.40.De
72.15.Eb
73.61.At

Keywords:
Transition metal alloys and compounds
Intermetallics
Thin films
Vapour deposition
Crystal structure
Electrical transport
Thermal expansion
X-ray diffraction

ABSTRACT

The thermal expansion coefficients (TEC) of metastable disordered intermetallic Fe–Cr phases formed in thin Fe–Cr alloy films prepared by an extremely non-equilibrium method of the pulsed laser deposition are studied. The lattice parameters of the alloys calculated from the low-temperature wide-angle X-ray diffraction (WAXRD) patterns show linear temperature dependencies in the temperature range 143–293 K and a deviation from the linearity at lower temperatures. The linear thermal expansion coefficients determined from the slopes of the linear portions of the temperature-lattice parameter dependencies differ significantly from phase to phase and from the values expected for the body-centered cubic (b.c.c.) $Fe_{1-x}Cr_x$ solid solutions. Strain-crystallite size analysis of the samples is performed. Predictions about the Debye temperature and the mechanical properties of the alloys are made.

1. Introduction

The Fe–Cr alloys are of a great interest due to their magnetic and structural properties. The stable Fe–Cr system has a large miscibility gap below 830 °C and a stable intermetallic σ-phase at nearly equiatomic alloy composition. However, by rapid cooling, disordered body-centered cubic (b.c.c.) Fe_xCr_{1-x} solid solutions with α-Fe-like structure can be easily produced in the whole composition range at room temperature (RT).

The rapid condensation from the gas phase promotes the formation of further metastable crystal structures in the Fe–Cr system at RT [1–7]. Especially the high quenching rate of the film material of the order of 10^{11} K/s in the pulsed laser deposition (PLD) [8] favors the formation of transient metastable material phases. These are α-Fe-like body-centered tetragonal (b.c.t.) phase in composition ranges $x = 0.26...0.37$ and $0.57...0.83$, γ-Fe-like face-centered orthorhombic (f.c.o.) phase at $x = 0.35...0.40$ and Cr_3Si-like primitive orthorhombic (p.o.) and primitive cubic (p.c.) phases in the Cr atomic-concentration range $x = 0.40...0.71$ [9,10]. The metastable f.c.c. and p.c. phases were found also in the mechanically-alloyed Fe–Cr powder mixtures [11].

This rich phase behavior in the Fe–Cr system has an immediate impact on the physical properties, which are sensitive to crystallographic features of the alloys. In the previous papers [12,13] we have reported that the remnant magnetization of the PLD Fe–Cr films starts decreasing with the onset of the tetragonal distortion of the b.c.c. structure until the $Fe_{1-x}Cr_x$ alloy becomes completely paramagnetic at $x = 0.27$ (according to table data, the undercooled b.c.c. Fe–Cr solid solutions become paramagnetic at RT at $x > 0.67$). A non-monotonous dependence of the electrical resistivity of Fe–Cr alloys on the composition has been studied in [14]. A pronounced minimum at nearly equiatomic composition was attributed to

* Corresponding author. Tel.: +49 351 4622740; fax: +49 351 4622168.
E-mail address: gorbunoff@mw.htw-dresden.de (A. Gorbunoff).

0925-8388/$ – see front matter © 2008 Elsevier B.V. All rights reserved.
doi:10.1016/j.jallcom.2008.10.039

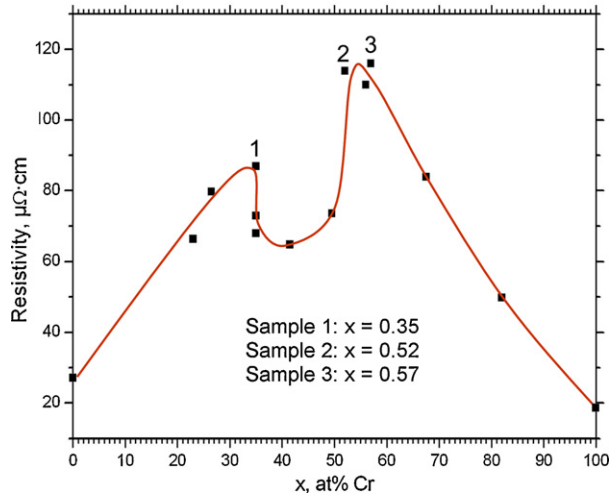

Fig. 1. The electric resistivity of Fe–Cr alloys fabricated by CBPLD. The samples used for the thermal expansion investigations are marked with numbers.

the partial ordering of the alloys, which was also noticed in ref. [12].

In the present paper we present data on the thermal expansion coefficients (TEC) of the metastable disordered Fe–Cr alloys fabricated by PLD.

2. Experimental

Samples of Fe–Cr alloys $10 \times 20\,mm^2$ in size and 40 nm thick were deposited on thermally oxidized (0 0 1) Si substrates by the cross-beam PLD (CBPLD) in vacuum. CBPLD is a particular variant of PLD with two colliding ablation plumes from simultaneously laser irradiated targets of individual metals. By variation the irradiation geometry, the samples with different compositions can be fabricated. The irradiation conditions were typical for CBPLD [8]. The main interest was addressed to the compositions in the middle concentration range, where the formations of the metastable phases are expected [10,14].

The electric resistivity of the samples served as an indication of the ordered phase formation. It was performed by a 4-point probe technique (RM3-AR, Jandel Engineering Ltd., UK) with 1 mm separated tungsten carbide probes (100 μm tip radius, 100 g spring load, 10 mA measurement current) in a linear arrangement. The measurements were taken in the middle of the samples at RT.

The samples deposited were studied by means of wide-angle X-ray diffraction (WAXRD) in high vacuum below 5×10^{-4} Pa. The WAXRD patterns were recorded in the relative coupled ω–2θ scan mode ($\omega = \theta + \Delta\omega$, offset $\Delta\omega = 0.5$–2° for different samples) using an X-ray diffractometer D5000 (Siemens AG, Germany; Bragg-Brentano geometry, scintillation detector, characteristic Cu-K_α radiation monochromatized by Johansson-type graphite monochromator) equipped with a cryostat chamber (Anton Paar KG, Austria). The offset $\Delta\omega$ is introduced to decrease the intensity of the Si substrate 0 0 4 reflection.

The control of the temperature (with an accuracy of ±0.5 K) was performed by a temperature sensor (Lake Shore Cryotronics Inc., USA) mounted in contact to the sample holder. The measurements were carried out in the temperature range from RT (≈293 K) down to 23 K in steps of $\Delta T = 20 \ldots 50$ K and back to RT using the same procedure. A 20 min dwell time was allowed at every temperature step for temperature equilibration. After the temperature equilibration at every temperature level, a rocking curve was recorded to check and correct the θ–2θ coupling of the diffractometer. Additionally, the WAXRD measurements of a bare substrate were carried out for comparison and control.

Table 1
Quantitative results obtained by analysis of the WAXRD patterns. The estimated standard deviations e.s.d.'s are indicated in parentheses.

Sample	Resistivity, (μΩ cm)	Crystalline phase	Lattice parameter at 293 K (nm)	Crystallite size t (nm) at $T = 293 \ldots 23$ K/strain s (%) at $T = 293 \ldots 143$ K[i]	$\alpha \times 10^{-6}$ (K^{-1}) experimental/corrected on strain[a]	$\alpha \times 10^{-6}$, (K^{-1}) calculated[b]
Si-substrate		f.c.c.	$a = 0.54305$[d]	–/–	2.0 (1)/–[f] 2.6[e]/–	–
Fe	27.2 9.98[d]	b.c.c.	$c = 0.28817(3)$[c] [§$a = 0.28665$[c]]	12.1(3)/0.1(1)[g,j]	11.8[d]/–[f]	–
Cr	18.7 12.7[d]	b.c.c.	$c = 0.29006(5)$[c] [$a = 0.28844$[c]]	39(6)/0.524(22)[g,j]	4.9[e]/–	–
$Fe_{0.65}Cr_{0.35}$	86.9	f.c.o.	$a = 0.3753(7)$ $b = 0.4089(5)$ $c = 0.4206(5)$	8.5(8)/0[m] 10.7(3)/0[n] 6.5(1.5)/0[p]	34.6(5.0)/34.6(5.0) 10.8(1.4)/10.8(1.4) 6.0(2.6)/6.0(2.6)	9.2
$Fe_{0.48}Cr_{0.52}$	114	p.c. p.o.	$c = 0.4638(2)$[c] $a = 0.4601(4)$ $b = 0.4638(4)$ $c = 0.4848(12)$	32(2)/0.349(6)[k] 8.2(1.1)/0[l] 32(2)/0.349(6)[k] –[f]	11.5(6)/11.5(6) 7.4(10.4)/7.4(10.4) 11.5(6)/11.5(6) –[f]	8.2
$Fe_{0.43}Cr_{0.57}$	116	p.c. p.o. b.c.t./b.c.c.	$c = 0.4646(4)$[c] $a = 0.4601(4)$ $b = 0.4646(4)$ $c = 0.4837(6)$ $c = 0.2899(4)$[c]	26(3)/0.514(9)[k] 18(4)/0.645(33)[l] 26(3)/0.514(9)[k] –[f] 39/0.439(24)[h,j]	15.0(2.1)/14.9(2.1) 10.7(6.7)/10.7(6.7) 15.0(2.1)/14.9(2.1) –[f] 12.8(8)/12.7(8)	7.9

[a] Determined from the slope of the linear temperature dependence of corresponding lattice parameter p in a temperature range 143–293 K according to equation $p(T) = p_{293}(1 + \alpha\Delta T)$, where p_{293} is a value of the lattice parameter at 293 K and $\Delta T = T - 293$ K. Correction of the lattice parameters on strain s (in %, see Fig. 3(b) and (c)) is performed according to equation $p_{corr}(T) = p(T)/(1 + s(T)/100)$.

[b] The thermal expansion coefficient of the unit cell parameter calculated for b.c.c. $Fe_{1-x}Cr_x$ compound according to equation $\alpha_a^{calc} = \alpha_a^{Fe}(1 - x_{Cr}) + \alpha_a^{Cr}x_{Cr}$.

[c] For cubic phases equivalent to unit cell parameter a.

[d] Table data [22].

[e] Table data [23].

[f] No data.

[g] At $T = 293$ K.

[h] Crystallite size t is fixed at the value determined for pure Cr film (based on the close values of the FWHM of the 110 reflections of the b.c.c. Cr and b.c.t. phase of $Fe_{0.43}Cr_{0.57}$).

[i] The e.s.d.'s of t and s characterize the scattering of the individual data obtained at different temperatures T according to the mean values indicated.

[j] [1 1 0]-b.c.c. (b.c.t.) crystallites.

[k] [0 1 0]-p.o. ([100]-p.c.) crystallites.

[l] [1 0 0]-p.o. crystallites.

[m] [1 1 1]-f.c.o. crystallites.

[n] [0 1 0]-f.c.o. crystallites.

[p] [0 0 1]-f.c.o. crystallites.

The WAXRD patterns recorded were analysed using programme ANALYZE [15]. The following reflections were used for the analysis: 1 1 0 and 2 2 0 (b.c.c., pure metals); 1 1 1, 2 2 2, 0 2 0, 0 4 0, 0 0 2 (f.c.o.); 2 0 0, 4 0 0, 0 2 0, 0 4 0 (p.o.). For every temperature level the central-angle Bragg $2\theta_B$ positions of the selected reflections of crystalline phases, their maximum and integral intensities, integral breadths β and the full width at half maximum (*FWHM*) were determined several times with different starting values. The averaged values of the parameters and their estimated standard deviations (e.s.d.'s) were obtained by averaging these individual values. The central-angle $2\theta_B$ positions of the reflections were used for least-square calculation (or refinement) of the corresponding lattice parameters of crystalline phases by means of a programme CellSize [16]. During the calculation/refinement, the 0 0 4 Si reflection of the substrate was used as an external standard for angle-corrections of the WAXRD patterns.

3. Results and discussion

The electrical resistivity ρ is a property which is quite sensitive to structural perfection of materials. It was studied first to select the proper samples for further investigations. The dependence $\rho(x)$ is presented in Fig. 1. Generally, it follows the trend described in ref. [14]: as the concentration of the solute grows, the resistivity strongly increases due to the enhanced electron scattering at the impurity atoms (the Nordheim rule) and at the grain boundaries of progressively smaller crystallites. In the region of the $0.35 \leq x \leq 0.50$ it shows a pronounced minimum, which was attributed to the formation of partly ordered p.c./p.o. intermetallic compounds. In order to avoid any additional anisotropy effects connected with the ordering of the alloys, three samples with compositions $Fe_{0.65}Cr_{0.35}$ (f.c.o.), $Fe_{0.48}Cr_{0.52}$ (p.o./p.c.) and $Fe_{0.43}Cr_{0.57}$ (p.o./p.c. and b.c.t./b.c.c.) *outside* this "ordering region" were selected for the investigations of TEC. The resistivity of these alloys is presented in the Table 1.

According to X-ray investigations, the films turned to be polycrystalline. Fig. 2 presents a portion of typical WAXRD patterns enlarged for a better view as well as the whole measured 2θ range in the insets. It is evident that only certain groups of the reflections are seen: (e.g., hhh, $0k0$, $00l$ for f.c.o. phase and $0k0$, $h00$ for p.o. phase) which indicates a pronounced preferred orientation (texture) of the films. These reflections origin from lattice planes parallel to the substrate, for which, due to the presence of free surface, the mechanical strain (film stresses, substrate influence) is minimal. Nevertheless, the non-substrate reflections observed are rather broad (see Fig. 2(a) and (b) as an example).

As it is known, the broadening of the WAXRD reflection profiles can be caused by the influence of small-size incoherently diffracting crystallites formed in the materials during sample preparation. Additionally, dislocations, vacancies, interstitials, substitutionals and other imperfections result in strain formation in crystallites (microstrain) followed by an additional broadening the reflection profiles. Both the crystallite size and the strain broadening can be separated by WAXRD reflection profile analysis due to their different 2θ-angle dependencies. To estimate the out-of-plane strain s and crystallite size t, the integral breadth method was used (see e.g., ref. [17]).

Depending on the quantity $FWHM/\beta$ one can distinguish between the Lotentzian-type ($FWHM/\beta \leq 2/\pi = 0.63662$) and Gaussian-type ($FWHM/\beta \geq 2\text{-}(\ln(2))^{1/2}/\pi^{1/2} = 0.93949$) of the reflection broadening [18]. For the samples investigated the quantity $FWHM/\beta$ was higher than 0.85. It is close to the limit-value for Gaussian reflection profiles, so that the Gaussian–Gaussian approximation was used for the separation of the size $FWHM_{size}$ and the strain $FWHM_{strain}$ reflection profile broadening effects and estimation of t and s:

$$FWHM^2 = FWHM^2_{size} + FWHM^2_{strain}$$

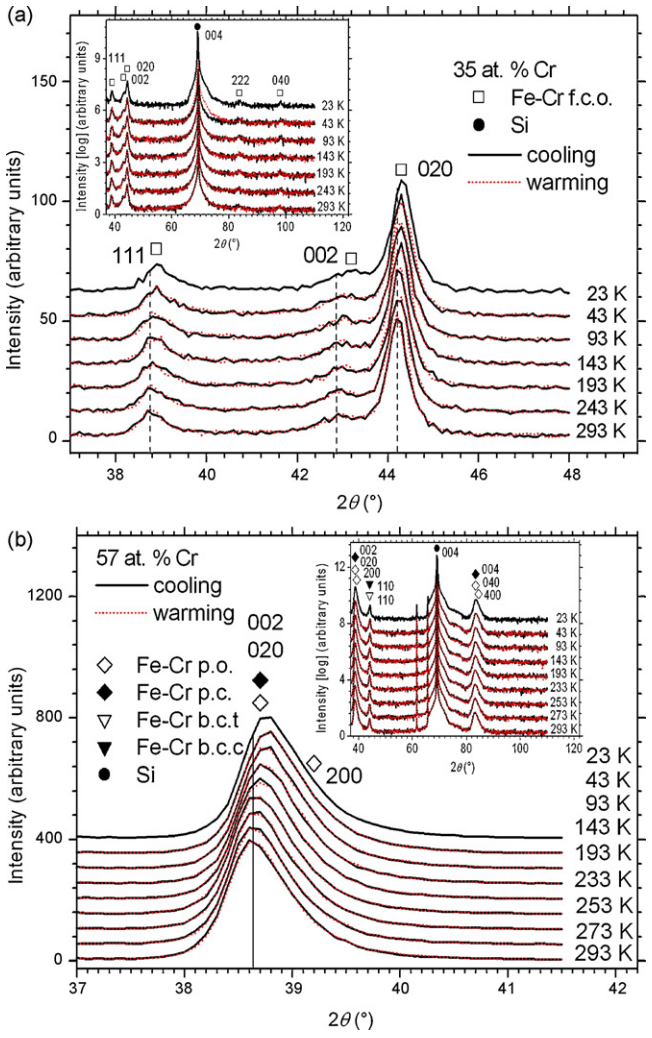

Fig. 2. A section of the WAXRD pattern of Samples $Fe_{0.65}Cr_{0.35}$ (a) and $Fe_{0.43}Cr_{0.57}$ (b) (offset $\Delta\omega = 1.0^\circ$ and 0.5°, respectively). The positions of the observed reflections of the crystalline phases are indicated at lowest temperature. For better visualization, the different WAXRD patterns are shifted and the central-angle position of the reflections at RT are marked by vertical dashed lines. Cooling (solid lines), warming (dotted lines). Insets show the WAXRD patterns in the whole 2θ-range measured.

The crystallite-size component of the WAXRD reflection profile broadening is estimated by Scherrer formula [19]:

$$FWHM_{size} = K\lambda/(t\cos(\theta_B)),$$

where $K = 0.94$ [20] for *FWHM*, λ is wavelength of the X-ray radiation used and t is crystallite size. For the strain contribution to the broadening the reflection profiles is calculated as:

$$FWHM_{strain} = K_{strain} s \tan(\theta_B),$$

where $K_{strain} = 4$ for the microstrain in crystallites [21].

The experimental *FWHM* was corrected to instrumental broadening $FWHM_{instr}$ using corresponding valid approximation for the instrumental reflection profile. $FWHM_{instr}$ was estimated at every temperature level using the results of the low-temperature WAXRD investigation of the (0 0 1) Si wafer. First, an assumption was made that both strain and crystallite size effects contribute to the reflection profile broadening (model '$t+s$'). For every temperature, the strain and crystallite size were calculated. As was expected, the crystallite sizes of all crystalline phases do not show a temperature dependence but scatter around a mean value (see an example in

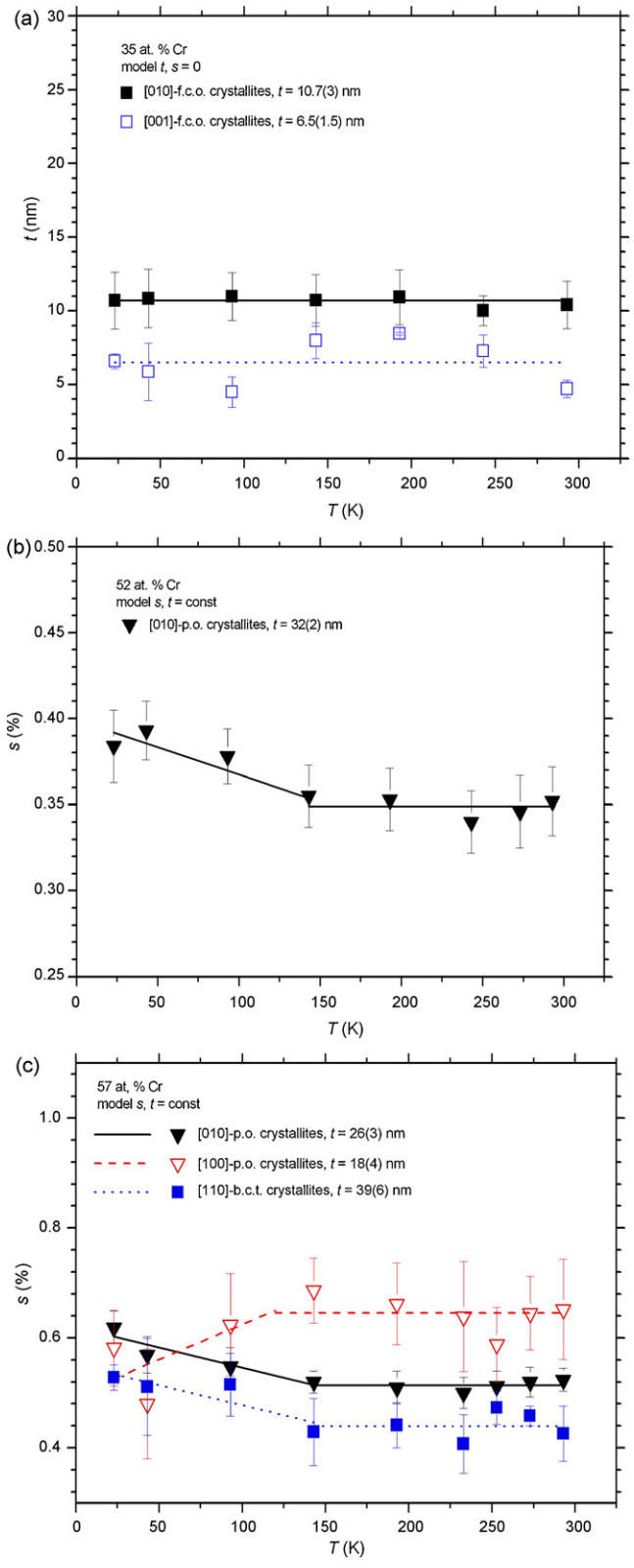

Fig. 3. The temperature dependencies of the size (a) and strain ((b) and (c)) for crystallites of Fe–Cr phases observed in (a) $Fe_{0.65}Cr_{0.35}$; (b) $Fe_{0.48}Cr_{0.52}$; (c) $Fe_{0.43}Cr_{0.57}$.

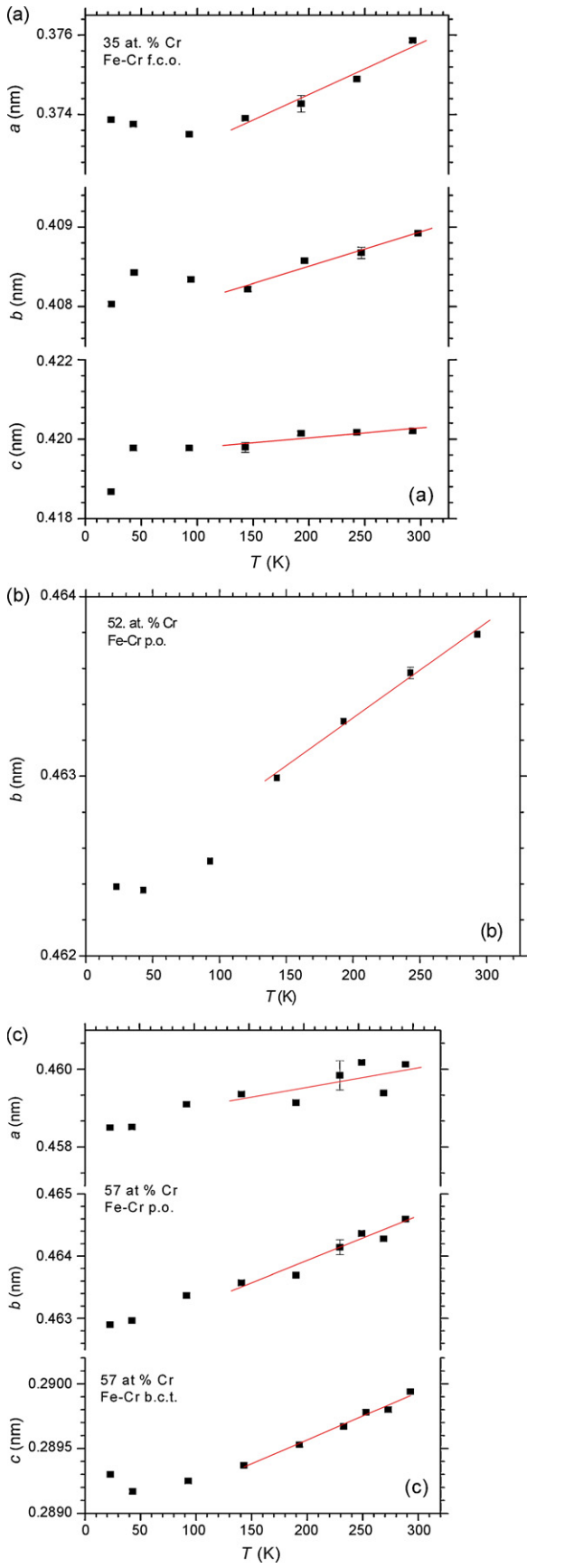

Fig. 4. The temperature dependencies of the lattice parameters of Fe–Cr phases observed in alloys studied. The linear least square fits in temperature ranges 143–293 K are shown. (a) $Fe_{0.65}Cr_{0.35}$; (b) $Fe_{0.48}Cr_{0.52}$; (c) $Fe_{0.43}Cr_{0.57}$.

Fig. 3(a)). At the next step of the calculations, the crystallite size was fixed at the averaged value and strain was recalculated (model 't, s = const').

As is seen in the Table 1 and Fig. 3, the size and strain in crystallites is orientation-dependent. The f.c.o. crystallites in $Fe_{0.65}Cr_{0.35}$ and [1 0 0]-p.o. crystallites in $Fe_{0.43}Cr_{0.57}$ film occurred to be rather small (t < 11 nm (Table 1)). The calculations for these crystallites with the assumption of strain were not successful so that no strain in these crystallites was assumed (model 't, s = 0')). Probably, the microstrain in smaller crystallites is relaxed due to the smaller surface area.

The reflection positions measured show the general trend to shift to higher angles with the decreasing temperature. No differences (within the experimental error) in the central-angle position and the shape of the reflection profiles during cooling and warming cycles were detected. The corresponding lattice constants (without correction to strain influence) vs. temperature are presented in Fig. 4. At the temperatures below 100 K, some anomalies in the behaviour of the lattice constants become apparent. Since the Curie temperature of the alloys lies also below 100 K [12,14], one can attribute these anomalies to the contribution of the magnetic component of the thermal expansion, whereas the local minimum in the expansion coefficient corresponds roughly to the Curie point of the alloy [24].

In the temperature region 143. . .293 K the lattice parameters increase practically linear with temperature. Note that a constant value of strain is observed in this temperature region (Fig. 3(b) and (c)). The linear TEC α determined from the slopes of the corresponding dependencies in this temperature region are summarized in Table 1. It is evident that TEC for each individual phase depend on the crystallographic directions and are influenced by the coexisting phases. In the most cases TEC of the alloys exceed the ones for the pure Fe and Cr and their b.c.c. alloys.

Since the Curie point of the alloys investigated lies far below T = 143 K, one can assume that only the lattice contribution dominate TEC at this temperature region. In the frames of the Debye–Grüneisen model [25], which assumes the weak temperature dependence of the bulk modulus (supported experimentally for many materials), it is temperature-dependent only below the Debye temperature T_D. Practically, the temperature independence of α is observed at $T > 0.5\ T_D$ [26]. From this observation one can conclude that the Debye temperature of the alloys studied lies at least below the RT (compare T_D (Fe) = 470 K, T_D (Cr) = 630 K [27]). Since T_D itself is connected to the bond elasticity, the alloys should be rather soft as compared to the pure constituent metals.

4. Conclusions

1. The linear TEC of disordered metastable f.c.o., p.c, and p.o. phases in the Fe–Cr system are determined for the first time.
2. TEC appear to be dependent on the phase, crystal orientation and coexisting phases and exceed in the most cases the ones for pure constituent metals and their b.c.c. alloys.
3. The temperature independence of TEC is reached well below the room temperature, which is an indication of relatively low Debye temperature and softness of the alloys.

References

[1] J.B. Kortright, S.-K. Kim, H. Ohldag, Phys. Rev. B61 (2000) 64–67.
[2] M.C. Simmonds, R.C. Newman, S. Fijitomo, J.S. Collington, Thin Solid Films 279 (1996) 4–6.
[3] K. Kimoto, I. Nishida, J. Phys. Soc. Jpn. 22 (1967) 744–756.
[4] C.J. Doherty, J.M. Poate, J.H. Voorhoeve, J. Appl. Phys. 48 (1977) 2050–2054.
[5] N. Yukawa, M. Hida, T. Imura, M. Kawamura, Inst. Met. J. 34 (1970) 348–355 (in Japanese).
[6] E. Le Bourhis, P. Goudeau, J.-P. Eymery, W. Al-Khoury, Eur. Phys. J. Appl. Phys. 30 (2005) 33–39.
[7] W. Al-Khoury, J.-P. Eymery, Ph. Goudeau, J. Appl. Phys. 102 (2007) 043511.
[8] A. Gorbunoff, in: R. Eason (Ed.), Pulsed Laser Deposition of Thin Films, Wiley, Hoboken, New Jersey, 2006, pp. 131–160.
[9] A.A. Levin, D.C. Meyer, A. Tselev, A. Gorbunov, W. Pompe, P. Paufler, J. Alloys Compd. 334 (2002) 159–166.
[10] A.A. Levin, D.C. Meyer, A. Gorbunov, A. Mensch, W. Pompe, P. Paufler, J. Alloys Compd. 360 (2003) 107–117.
[11] F.Z. Bentayeb, S. Alleg, B. Bouzabata, J.M. Grenèche, J. Magn. Magn. Mater. 288 (2005) 282–296.
[12] A. Gorbunov, A.A. Levin, A. Mensch, D.C. Meyer, A. Tselev, P. Paufler, W. Pompe, D. Eckert, Appl. Surf. Sci. 197–198 (2002) 475–480.
[13] E. Wieser, H. Reuther, F. Prokert, A. Gorbunov, A. Tselev, W. Pompe, A.A. Levin, D.C. Meyer, P. Paufler, J. Appl. Phys. 92 (2002) 572–577.
[14] A. Gorbunov, A.A. Levin, D.C. Meyer, L. Bischoff, D. Eckert, B. Köhler, M. Mertig, T. Weiβbach, E. Wieser, W. Pompe, Cryst. Res. Technol. 40 (2005) 106–113.
[15] Programm ANALYZE, Rayflex Version 2.285, Rich. Seifert & Co. (2000).
[16] Programm Celsize, Version 1.1, freeware available via Homepage of International Union of Crystallography (1995).
[17] K. Santra, P. Chatterjee, S.P. Sen Gupta, Bull. Mater. Sci. 25 (2002) 251–257.
[18] J.I. Langford, Accuracy in Powder Diffraction, National Bureau of Standards, Special Publication No. 567, 1980, pp. 255–269.
[19] R.A. Young, A. Sakthivel, T.S. Moss, C.O. Paiva-Santos, J. Appl. Cryst. 28 (1995) 366–367.
[20] J.I. Langford, J. Appl. Cryst. 11 (1978) 10–14.
[21] R. Stokes, A.J. Wilson, Proc. Phys. Soc. Lond. 56 (1944) 174–181.
[22] O. Villars, L.D. Calvert, Pearson's Handbook of Crystallographic Data for Intermetallic Phases, American Society for Metals, Metal Park, OH, 1991.
[23] D.R. Lide (Ed.), CRC Handbook of Chemistry and Physics, 86th ed., CRC, Boca Raton, Florida, 2005.
[24] V.E. Rode, A.I. Lyalin, S.A. Finkelberg, J. Appl. Phys. 52 (1982) 8122–8124.
[25] L.D. Landau, E.M. Lifshitz, Statistical Physics, 3rd ed., Butterworth-Heinemann, Oxford, 1980, Pt. 1.
[26] G. Gottstein, Physikalische Grundlagen der Materialkunde, 3, Springer-Verlag Berlin Heidelberg, Auflage, 2007.
[27] C. Kittel, Introduction to Solid State Physics, 7th ed., John Wiley & Sons, New York, Chichester, 1996.